Cell Transplantation
Volume 34: 1–14

DOI: 10.1177/09636897251342462
journals.sagepub.com/home/cll
Sage

The safety and efficacy of ultrasound histotripsy and human pluripotent stem cell–derived hepatic spheroid implantation as a potential therapy for treatment of congenital metabolic liver disease: Assessment in an immunocompetent rodent model

Hassan Rashidi[1*], Amjad Khalil[2,3,4*], Saied Froghi[3*], Andrew Hall[5], Pierre Gelat[6], Brian Davidson[2,3,4], Alberto Quaglia[5], and Nader Saffari[7]

Abstract

Liver disease secondary to an inborn or genetic error of metabolism is a rare group of conditions often associated with chronic ill health and reduced survival. Curative treatment is mainly limited to liver transplantation with major long-term risks. Cell therapy is a promising alternative, but current approaches are ineffective. To develop histotripsy, a non-invasive high-intensity ultrasound procedure for liver tissue mechanical ablation, combined with hepatocyte stem cell implantation as a novel method of reversing liver failure from genetic disease. This study assessed the safety and feasibility of this approach in healthy rodents. Under general anaesthesia, adult rats (n = 12) underwent laparotomy and ultrasound histotripsy to the exposed liver. Around 1 million cells were injected into a single histotripsy cavity in each animal under direct vision (n = 10) with two receiving only histotripsy without cell injection. On completion of cell implant, haemostasis was secured, laparotomy incision closed and the animals recovered. Groups of animals were terminated immediately and after 4 h, 8 h, 24 h, 4 days and 7 days. Liver and vital organs were assessed for procedure-related injuries and evidence of viable implanted cells by histology and immunohistochemistry. All animals successfully recovered, and no complication was observed throughout the study. Created cavities were successfully identified in histological analysis of rat. The presence of human cells was verified using anti-human nuclei antibody confirming successful implantation of liver organoids into decellularised cavities. In this feasibility study, we demonstrated suitability of histotripsy to create decellularised cavities in liver parenchyma. In addition, feasibility of direct transplantation of undissociated liver organoids into the created cavities was demonstrated as a potential approach to treat inborn liver disease by creating nodules of healthy cells capable of performing loss metabolic function. Therapeutic efficacy of this approach will be evaluated in an upcoming study.

Keywords

liver cell transplantation, histotripsy, human pluripotent stem cell–derived liver organoids

[1]Great Ormond Street Institute of Child Health, University College London, London, UK
[2]Liver Unit, The Wellington Hospital, London, UK
[3]Centre for Surgical Innovation, Organ Regeneration and Transplantation, University College London, London, UK
[4]Clinical Service of HPB Surgery and Liver Transplantation, Royal Free Hospital, London, UK
[5]Cancer Institute, University College London, London, UK
[6]Division of Surgery and Interventional Science, University College London, London, UK
[7]Department of Mechanical Engineering, University College London, London, UK

*These authors contributed equally.

Received: 12 November 2024; revised: 19 April 2025; accepted: 23 April 2025

Corresponding Author:
Hassan Rashidi, Great Ormond Street Institute of Child Health, University College London, 30 Guilford Street, London WC1N 1EH, UK.
Email: h.rashidi@ucl.ac.uk

Graphical Abstract

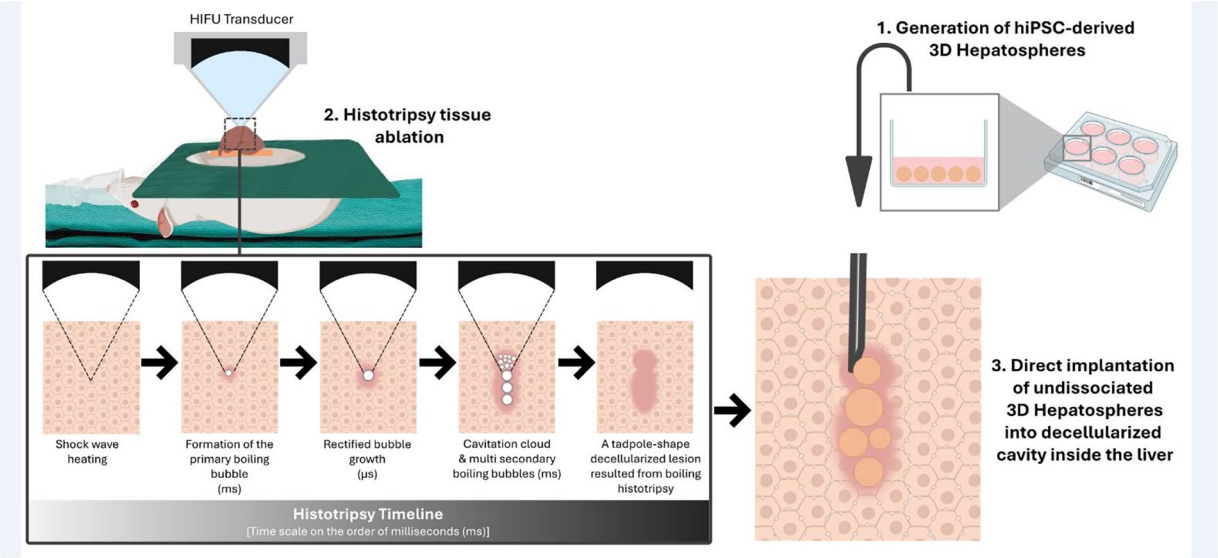

Introduction

Congenital liver diseases are diverse group of genetic disorders that primarily affect liver function from birth. These conditions can lead to significant morbidity and mortality due to liver dysfunction resulted from accumulation of toxic metabolites[1]. Inborn metabolic disorders are rare but remain an important cause of liver disease[2]. Liver transplantation (LT) is one of the few effective treatments but is associated with a significant mortality in children (~5% within the first year) and with a high risk of post-transplantation complications (up to 70%). In addition, there is a shortage of suitable donor organs for children, a risk of rejection and a requirement for life-long immunosuppression treatment which is associated with increased risk of sepsis, *de novo* cancer and renal failure[3].

Alternative approaches have been sought to overcome limitations associated with LT including pharmacological interventions, gene therapy and cell therapy[4,5]. Cell therapy can be used as a curative option in metabolic disorders or as a bridge to transplantation[3]. Primary human hepatocytes (PHHs) have been considered as the optimum cell source for transplantation but represent a limited resource[6].

Human pluripotent stem cells (hPSCs) possess unique features including the ability to be expanded indefinitely and the potential to be differentiated into any cell type found in the human body, making them an attractive source for cell therapies[7]. To this end, various approaches have been developed to generate functional hepatocytes from hPSCs as a renewable source[8–13].

Several approaches have been used for cell implantation into the liver or ectopically into other organs such as the spleen, peritoneal cavity and lymph nodes[14–17]. Endovascular infusion, particularly into the portal vein, has been the preferred and most common route for hepatocyte transplantation in a clinical setting[18]. Embolism of terminal radicals of the portal system following transfusion of hepatocytes and subsequent vascular permeabilisation has been suggested as the potential mechanism of cell integration. The embolism leads to portal hypertension, triggering the release of vasculature permeabilisation cytokines from Kupffer and stellate cells that facilitate integration of transplanted cells into the liver parenchyma[19]. The engraftment efficiency is low at 5% to 30% as most of the non-integrated hepatocytes that remain wedged in the portal vessels are cleared by macrophages within 24 h[20]. The engraftment efficiency can be enhanced following preconditioning treatment of the liver by disruption of the sinusoidal endothelium, administration of vasodilators, inhibition of macrophage function and irradiation though most of these strategies are not clinically acceptable[20–23]. Therefore, development of novel cell engraftment methodologies is a necessity in the field of liver cell therapy.

Ultrasound histotripsy can be used to mechanically fractionate soft tissues with a high degree of precision and has been used for non-invasive ablation of solid tumours[24,25]. To develop an efficient and targeted transplantation methodology, a protocol known as boiling histotripsy was previously used by our group to create well-defined decellularised cavities in rat liver without any noticeable thermal damage[26].

The aim of this study was to use our previously developed US histotripsy protocol with the inclusion of a pulse-echo ultrasound transducer to generate a liver cavity in which to transplant undissociated hPSC-derived 3D Hepatospheres (3D-Heps) and to determine the feasibility and safety of this approach as a potential treatment for congenital metabolic liver disease.

Materials and methods

Animals

Mature Male Sprague Dawley rats, weighing 430–530 g, were obtained from the Charles River Laboratories UK Ltd (Margate, Kent, UK). The animals were housed in a temperature-controlled room (19°C–24°C), with a relative humidity of 40%–70% and alternate light/dark conditions. They were given standard laboratory rodent chow. All animal experiments were conducted according to the Home Office guidelines under the UK Animals and Scientific Procedures Act 1986. All experiments were done under isoflurane general anaesthesia.

Maintenance of human-induced pluripotent stem cells

An inhouse-generated human-induced pluripotent stem cell (hiPSC) line (GOS101B) was used in this study. GOS101B was cultured on laminin 521 (BioLamina)-coated plates in serum-free mTeSR1 medium (STEMCELL Technologies) as previously described[27]. The cell lines were propagated in antibiotic-free medium and were monitored regularly for mycoplasma infection using MycoAlert PLUS Mycoplasma Detection Kit (Lonza, Switzerland).

Generation of self-aggregated hiPSC spheroids

A previously published protocol was used to generate 3D Heps from hPSCs[28]. Initially, agarose microplates were fabricated in 256-well format using the MicroTissues 3D Petri Dish mold (Sigma Aldrich, USA) following the manufacturer's instructions and transferred to 12-well plates (Corning, USA). hPSCs scaled up on laminin-coated plasticware and were incubated with 1 ml of Gentle Dissociation Buffer (STEMCELL Technologies, Canada) for 7 min at 37°C. Following this, single-cell suspensions were prepared by pipetting the buffer up and down gently. The cell suspension was centrifuged at 0.2 relative centrifugal force (rcf) for 5 min, discarded the supernatant and resuspended in mTeSR1 supplemented with 10 μM Y-27,632 (Cayman Chemical Company, USA) at a density of 2.0×10^6 live cells/ml. The agarose microplates were seeded by transferring 190 μl of cell suspension. After 2–3 h, 1 ml of mTeSR1 supplemented with 10 μM Y-27,632 was gently added to each well of the 12-well plate and incubated overnight to allow formation of self-aggregated spheroids as described elsewhere[28].

Differentiation into 3D Heps

Differentiation was initiated a day after generation of hiPSC spheroids by replacing mTeSR1 with endoderm differentiation medium which consisted of RPMI 1640 containing 1 × B27 (Life Technologies, UK), 100 ng/ml Activin A (PeproTech, USA) and 50 ng/ml Wnt3a (R&D Systems, USA). The medium was changed every 24 h for 72 h. On day 4, the endoderm differentiation medium was replaced with a hepatoblast differentiation medium. The medium consisted of KnockOut (KO)-DMEM (Life Technologies, UK), KnockOut Serum Replacement (KOSR; Life Technologies, UK), 0.5% Glutamax (Life Technologies, UK), 1% non-essential amino acids (Life Technologies, UK), 0.2% b-mercaptoethanol (Life Technologies, UK) and 1% DMSO (dimethyl sulfoxide) (Sigma, USA), and was renewed every second day for a further 5 days. On day 9, the medium was replaced by a hepatocyte maturation medium HepatoZYME (Life Technologies) containing 1% Glutamax (Life Technologies, UK), supplemented with 10 ng/ml hepatocyte growth factor (HGF; PeproTech) and 20 ng/ml oncostatin M (PeproTech, USA). On day 21, cells were cultured in a maintenance medium consisting of William's E media (Life Technologies, UK), supplemented with 10 ng/ml EGF (R&D Systems, USA), 10 ng/ml VEGF (R&D Systems, USA), 10 ng/ml HGF (PeproTech, USA), 10 ng/ml bFGF (PeproTech, USA), 10% KOSR, 1% Glutamax and 1% penicillin–streptomycin (Thermo Fisher Scientific, USA).

Immunofluorescence staining

Prior to implantation, 3D Heps were fixed in ice-cold methanol for 30 min, washed in phosphate-buffered saline (PBS) and embedded in agarose before embedding in paraffin to obtain sections of 4 μm thickness. Antigen retrieval was performed by heating dewaxed and rehydrated sections in 1× Tri-sodium Citrate buffer solution for 15 min in a microwave oven using defrosting option to avoid boiling of the buffer. Washed slides were used for subsequent staining to characterise generated cells.

To perform immunostaining, stem cell–derived tissue was blocked with 10% bovine serum albumin (BSA) in PBS–Tween (PBST) and incubated with primary antibody overnight at 4°C and detected using species-specific fluorescent-conjugated secondary antibody (Alexa Flour 488/Alexa Flour 568/Alexa Flour 680; Invitrogen). Sections were counterstained with DAPI (4′,6-diamidino-2-phenylindole) and mounted with ClearMount mounting solution (Invitrogen, USA).

An extended staining protocol was developed and optimised to stain whole mount 3D Heps. Briefly, MeOH fixed spheroids were washed and rehydrated in PBS. Following overnight blocking in 10% BSA in PBST, the spheroids were incubated with primary antibody at desired concentration (Supplementary Table 1) with gentle agitation at 4°C overnight followed by eight washes with 0.1% PBST (each wash 1 h) under gentle agitation at room temperature (RT). Secondary antibodies were incubated at 4°C overnight and washed as described above. The nucleus was counterstained with DAPI (Life Technologies) before images were acquired using a Zeiss LSM 880 upright multiphoton confocal microscope.

Cytochrome P450 assay

3D Heps derived from hiPSCs were incubated for 1.5, 4 and 24 h, with the luciferin-conjugated specific CYP3A (1:40) substrate (P450 P-Glo Luminescence Kit; Promega) at 37°C. The Luciferin detection reagent was reconstituted by mixing the buffer into the bottle containing the lyophilised Luciferin detection reagent. For measurement, in a white 96-well plate, 50 µl of the supernatant sample mixed with 50 µl of the detection reagent was added and incubated at RT in the dark for 20 min. The data were collected using a luminometer (GloMax Navigator; Promega). For data analysis, units of activity were measured as relative light units per millilitre per microgram protein (RLU/ml/mg) as determined by the bicinchoninic acid (BCA) assay.

Gene expression analysis

Quantitative real-time polymerase chain reaction (qRT-PCR) was performed to demonstrate expression of the liver-specific genes HNF4A, ALB and CYP3A4. RNA was extracted from 3D Heps using the Direct-zol RNA Miniprep kit (Zymo Research, USA). RNA quantity and quality were assessed using a Nanodrop system. Following this, complementary DNA (cDNA) was amplified using the RevertAid First Strand cDNA Synthesis Kit (Thermo Fisher Scientific, USA) following the manufacturer's instruction. Quantitative PCR (qPCR) was performed with TaqMan Fast Advance Mastermix and primer pairs listed in Supplementary Table 2 and analysed using a CFX96 Real-Time PCR System (Bio-RAD, USA). Gene expression was normalised to glyceraldehyde 3-phosphate dehydrogenase (GAPDH) and expressed as relative expression over 3D aggregate on day 0 of differentiation as control sample. qPCR was performed in triplicate and data analysis was performed using manufacturer software and graphs were prepared using GraphPad PRISM software (version 10.1.2).

Enzyme-linked immunosorbent assay

3D Heps derived from hiPSCs were incubated with maintenance medium for 24 h at 37°C in 5% (v/v) CO_2, 95% (v/v) O_2. The supernatants were collected after 24 h. The markers of hepatocyte functionality, albumin (ALB) and alpha-fetoprotein (AFP) levels were measured, using human ALB and AFP DuoSet enzyme-linked immunosorbent assay (ELISA) kits (R&D Systems).

To detect human AFP and ALB in transplanted animals, 100 µl of plasma samples was loaded into pre-coated ELISA plate in duplicate followed by 1-h incubation at RT as per manufacturer's instructions. Following this step, microwells were washed with working wash solution for four times and diluted anti-human AFP or ALB horseradish peroxidase (HRP) conjugated was added to the microwells. The wells were incubated at RT for 30 min. Microwells were washed with working wash solution five times, and the substrate for the HRP enzyme tetramethylbenzidine (TMB) was added and incubated for 15 min in the dark. Following this step, the stop solution was added to each well and the plates' luminous activity was measured at 450 nm with a reference wavelength of 630 nm using a FLUOstar Omega plate reader (BMG LabTech, Germany). Plain tissue culture media which was incubated for 24 h at 37°C was employed as the negative control. For data analysis, the collected data were normalised per microlitre per microgram protein as measured by the BCA assay (Pierce, UK).

Development of ultrasound histotripsy treatment protocol

A 2-MHz single-element spherical section transducer (H-148; Sonic Concepts, Bothell, WA, USA) with an aperture size of 64 mm, a radius of curvature of 63.2 mm and a central aperture of 22.6 mm was used with a transparent coupling cone (C-101; Sonic Concepts) filled with degassed, deionised water. The cone was coupled directly to the animal's exteriorised liver via a 12-µm-thick acoustically transparent polyethylene (Mylar) film (PMX 980; HiFi Industrial Film, Stevenage, UK). The transducer was driven by two function generators (Agilent 33220A, CA, USA) connected in series to a linear radiofrequency (RF) power amplifier (ENI 1040L, Rochester, NY, USA). The first function generator was set to generate pulses of a 1-Hz rectangular wave with 1% duty cycle. This triggered the second function generator, which outputted a 2-MHz sinusoidal wave into the RF power amplifier. Therefore, the drive signal into the amplifier was 30 to 35 pulses of 10 ms duration containing 20,000 cycles each. A power metre (22A; Sonic Concepts) was connected between the RF amplifier and the ultrasound transducer, and the electrical power supplied to the transducer was monitored to be approximately 150 W (Supplementary Fig. 1). The pulse-averaged electrical power was 1.5 W (calculated using $P_{averaged} = P_{peak} \times$ duty cycle). Assuming a nominal electrical to the acoustic power conversion efficiency of 85% (Sonic Concepts), the acoustic peak positive (P+) and negative (P−) pressures at the ultrasound beam focus in liver tissue were $P+ = 76.7$ MPa and $P- = -13.4$ MPa, obtained by numerically solving the Khokhlov–Zabolotskaya–Kuznetsov (KZK) parabolic nonlinear wave propagation equation for our input parameters using the HITU Simulator v2.0[29]. These pressure distributions are shown in Fig. 1.

To ensure correct and consistent coupling between the cone and the liver surface, we inserted a pulse-echo transducer (Olympus V312, 10 MHz center frequency, 6 mm element diameter, unfocused) in the central open aperture of the Sonic Concepts H-148 transducer, as shown in Fig. 2. This transducer was connected to a Panametrics 5055PR

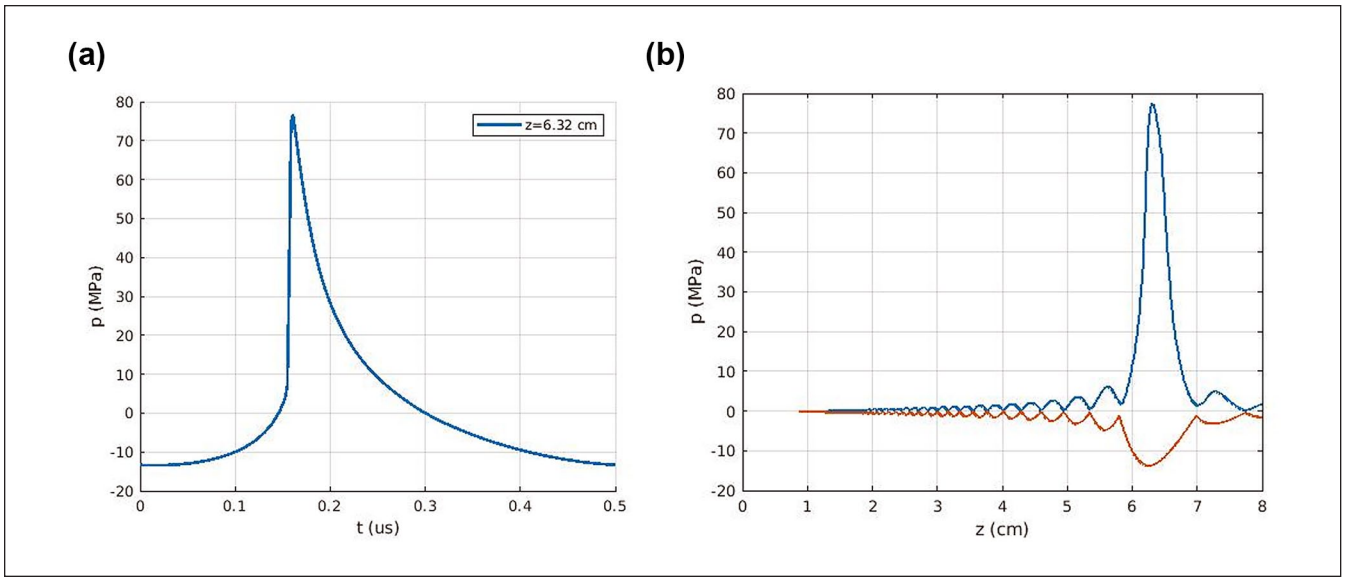

Figure 1. Numerically simulated ultrasound waveforms (a) at the geometrical focus of the transducer in liver tissue and (b) the axial distribution of the positive and negative peak pressure values.

pulser-receiver for the excitation and detection of the returned echoes from the surface of the liver.

Experimental design

Twelve animals were divided into six subgroups, each with distinct termination points. The non-recovery group consisted of four animals: two were sacrificed immediately post-histotripsy (histotripsy alone control), while the remaining groups were subjected to termination at various intervals post-3D hepatocyte transplantation: immediately (n = 2), 4 h (n = 2), 18 h (n = 2), 24 h (n = 2) and >24 h (4 days (n = 1) and 7 days (n = 1)) (Supplementary Table 1).

Surgical procedure

Male Sprague Dawley Rats (n = 12) were individually placed in an anaesthetic induction chamber. Flow of Isoflurane with oxygen was gradually increased until anaesthesia was induced. The animal was removed from the chamber, with anaesthesia maintained via a close-fitting mask. Animals were placed on a warm pad in theatre, abdominal hair clipped and skin cleaned with chlorhexidine. Two drops of 2% lidocaine were injected subcutaneously followed by an upper midline laparotomy incision. Skin and fascia were retracted using 4/0 prolene sutures and weighted down with mosquito forceps. The right median lobe of the liver was mobilised preferentially and placed on sterile gauze, outside the abdominal cavity producing an air gap to produce a larger ultrasound reflection for measuring the thickness of the liver lobe.

The histotripsy probe was then lowered onto the exposed liver, so the exit aperture of the coupling cone was in contact with the exposed area of the liver. The histotripsy parameters are mentioned in Supplementary Table 1. Once the histotripsy procedure was complete, the experimental group received 200 µl of cell suspension in saline buffer injected into the created cavity, whereas the control group received histotripsy only (see Fig. 2). To perform injection under control manner, a syringe pump was used to inject the volume at 1.2 ml/min. A haemostatic gelatin matrix, containing thrombin (SURGIFLO) was used to cover the cavity site in 3D Hep-implanted animals to prevent bleeding and leakage of implanted cells and it was applied on non-injected controls to keep procedure consistent between control and test groups. All animals underwent a single histotripsy procedure except animal 11 which underwent a second procedure as the presence of a cavitation haematoma was not observed after the initial sonification on the right median lobe. Following a check of haemostasis, the abdomen was closed in layers with interrupted vicryl 3/0 to the fascia and prolene 3/0 to the skin. Veterinary Wound Powder and Opsite were administered to the closed wound sites.

Non-recovery animals were terminated immediately post procedure with cardiac puncture for venous sampling followed by intra-cardiac overdose with sodium pentobarbitone. Immediately following termination, livers were harvested and immersed in formaldehyde solution, prior to paraffin fixation. Recovered animals were taken back to the animal accommodation area after a period of observation and received regular analgesia. Figure 2 outlines key procedures.

To examine creation of the cavity, cell transplantation and early onset of tissue repair, we sacrificed the animals immediately post-histotripsy (n = 2; only histotripsy control) and immediately (n = 2), 4 h (n = 2), 18 h (n = 2), 24 h (n = 2), 4 days (n = 1) and 7 days (n = 1) post-3D Heps transplantation.

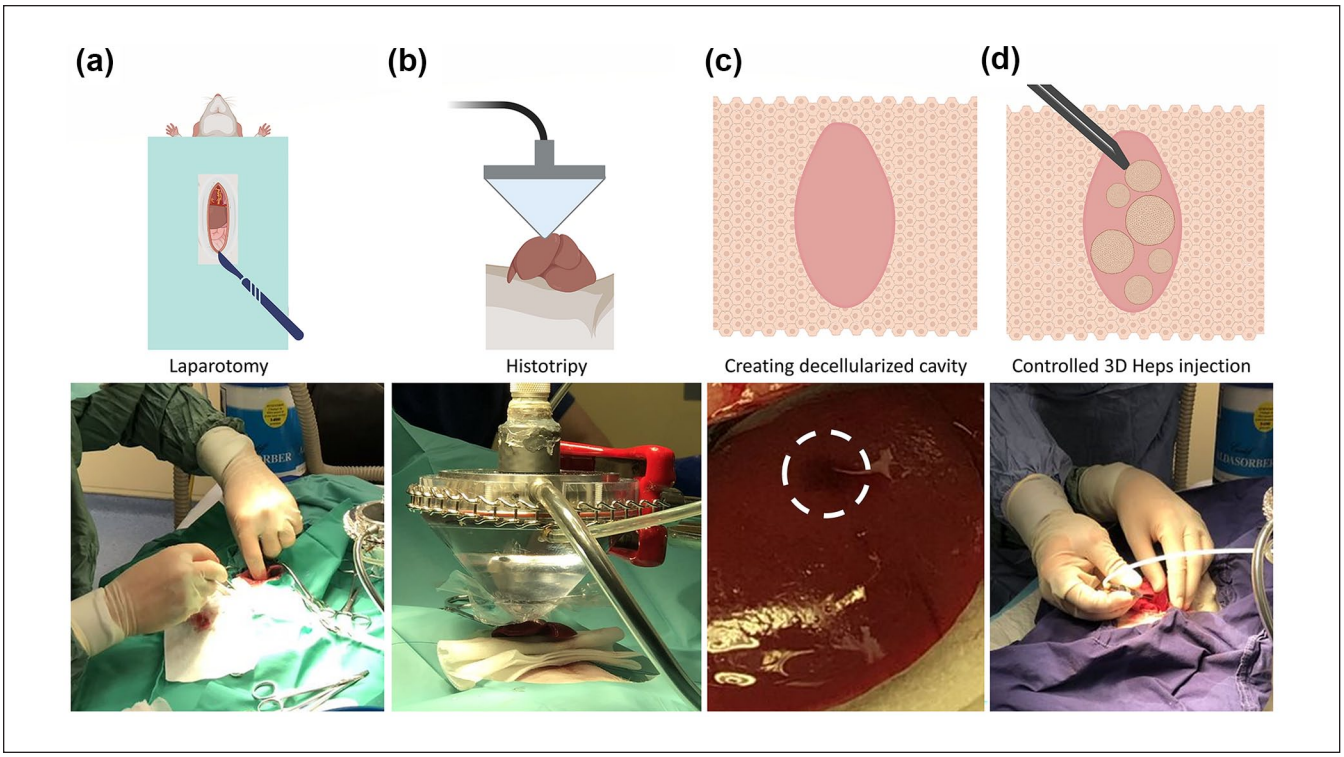

Figure 2. Histotripy decellularisation and cell transplantation. (a) Laparotomy to allow exteriorisation of the liver. (b) The histotripsy transducer was adjusted to touch the liver capsule lightly before initiating the protocol. (c) Creation of the cavity was confirmed visually following observation of haematoma under liver capsule (indicated with white dashed circle). (d) 3D Heps were administered using a syringe pump to permit controlled injection of the designated volume to avoid rupturing the liver.

Histology

Each liver was dissected into three to five slices and fixed for at least 24 h in 10% neutral buffered formalin solution (pH 7.4) at RT. Samples were subsequently processed into formalin-fixed paraffin-embedded (FFPE) blocks for preservation.

For each block, we took a set of seven serial sections of 4-µm thickness starting with the most superficial aspect and stained the first and last of the set of serial sections with haematoxylin and eosin (H&E). Sections were dewaxed in xylene and hydrated graded alcohols before staining for 10 min in Harris's haematoxylin (VWR cat no. 10047107). The slides were rinsed in tap water before differentiation in 1% acid (HCl) 70% alcohol (aqueous) before blueing in tap water for 5 min. The slides were counterstained with eosin (VWR cat no.10047101) for 5 min and then washed in running tap water for 1 min. The slides were then rapidly dehydrated, cleared and then mounted in DPX (VWR cat no 06522-500ML).

The H&E-stained slides were reviewed; if no cavity was seen, the block was trimmed 100 µm deeper and another seven serial sections were taken with the first and last being stained for H&E again for review. This procedure was repeated up to 14 times to identify any cavities throughout the tissue. Brightfield images were taken using a Hamamatsu NanoZoomer slide scanner.

Immunohistological analysis

When a suspected cavity was found, the reserved unstained serial sections between the stained H&E sections were stained with IHC Anti-Human Nucleoli antibody (NM95)—nucleolar marker for the detection of human nuclear antigen. Sections were dewaxed in xylene and hydrated in graded alcohols. Antigen retrieval was carried out (20 min microwave at 640W in 1 l of pH 6.0 citrate buffer) before endogenous peroxidases were blocked (Bloxall; Vector Laboratories, USA). Sections were incubated in 2.5% Horse serum (ImmPRESS Enzyme Polymer; Vector Laboratories, USA) for 5 min and then incubated for 1 h at RT in NM95 primary antibody (ab190710 16; Abcam, UK) at 1:1500 in Tris-buffered saline (TBS). Primary antibody binding was detected by incubating for 25 min in polymer solution (ImmPRESS Enzyme Polymer; Vector Laboratories, USA) and developed with 3,3′-diaminobenzidine (DAB, ab64238; Abcam, UK). Slides were counterstained in Mayer's haematoxylin before they were dehydrated, cleared and mounted. Brightfield images were taken using a Hamamatsu NanoZoomer slide scanner.

Statistical analysis

Data were analysed by GraphPad Prism (version 9.0). Student's *t* test or Mann–Whitney tests were used to

determine significant differences, which was set at $P < .05$. We did not use statistical methods to predetermine sample size, there was no randomisation designed in the experiments and the studies were not blinded.

Results

Generation of hPSC-derived 3D Heps and functional characterisation

Aggregated hPSCs were differentiated towards the hepatocyte lineage using a stepwise differentiation protocol described previously (Fig. 3a)[12]. To produce homogeneous three-dimensional spheres (3D Heps) of defined size, the agarose multi-well plate technology was employed to form hPSC aggregates. By day 30 of differentiation, 3D Heps exhibited typical hepatic morphology with distinctive cell borders which was maintained until harvesting the organoids for transplantation on day 60 of differentiation (Fig. 3a). Differentiation to hepatic lineage was confirmed following detection of liver-specific genes by qPCR (Fig. 3b). We also measured the level of AFP and ALB secretion using ELISA (Fig. 3c) and CYP3A4 metabolic activity (Fig. 3d). Finally, we performed immunostaining analysis of hepatic markers such as hepatocyte nuclear factor 4 alpha (HNF4A), AFP, ALB and CYP3A4 (Fig. 3e).

Termination of recovered animals

Recovered animals were terminated immediately after histotripsy and cell implantation (n = 2) and at 4 (n = 2), 18 (n = 2), 24 (n = 2), 96 (n = 1) and 168 h (n = 1) post cell implantation. Animals were terminated by placing the animals in an anaesthetic induction chamber, followed by a gradual increase in the flow of isoflurane. Once anaesthetised, a cardiac puncture was performed for venous sampling followed by intra-cardiac overdose with sodium pentobarbitone. Once death was confirmed, a postmortem laparotomy and sternotomy were performed with lateral subcostal extension on each animal. Livers were preferentially harvested and immersed in formaldehyde solution, prior to paraffin fixation.

Findings at postmortem

On macroscopic examination, animals terminated within 24 h (tests 3–8) were found to have clean and healthy incision wounds, a single cavity within the liver (marked with SURGIFLO) with minimal adherence to the diaphragm and abdominal wall. The livers appeared healthy, warm and well perfused. The remaining peritoneum and abdominal cavity appeared unremarkable, with no macroscopic, adhesions, haematoma, scarring, inflammation, injury or compensatory hypertrophy.

Animals terminated after 24 h (tests 9 and 10) had superficial wound dehiscence in the epigastric region of their laparotomy incisions, with the liver densely adhered to the incised abdominal wall and diaphragm with fibrous bands. The livers appeared healthy, warm and well perfused. The remaining peritoneum and abdominal cavity appeared unremarkable, with no macroscopic adhesions, haematoma, scarring, inflammation, injury or compensatory hypertrophy.

Histological analysis

Created histotripsy sites were identified in 1 out of the 2 histotripsy control animals and 4 out of 10 animals injected with 3D Heps (Fig. 4). In the control animal, the histotripsy site consisted of a flask-shape decellularised area, filled with cell debris and red blood cells (Fig. 4a–c) reaching a parenchymal depth of 4 mm below the liver surface and measuring 2 mm in maximum width. The histotripsy site reached the liver surface and was in contact with the Surgiflo gel plug without a visible interposed intact liver capsule at a point measuring 0.8 mm in diameter. The presence of 3D Heps in the form of cell aggregates was observed only in the livers implanted with cells (Fig. 4d–p), of test animals 1, 2, 4, 8 and 10. The histotripsy sites showed a combination of necrosis and haemorrhage in animals 1, 2, 4 and 8, similar in appearance to the histotripsy site in the control animal. Three of these sites (animals 2, 4 and 8) showed an elliptical shape and were of variable length (2, 1.2 and 3.6 mm) and width (0.5, 0.5 and 1.4 mm, respectively), in the sections examined. The histotripsy site in animal 2 was located 2 mm from the liver capsule, which appeared intact (Fig. 4d–f). A 1.2-mm × 0.5-mm separate subcapsular patch of necrosis and haemorrhage was also present. The histotripsy site in animal 4 was in contact with a 0.5-mm indentation of the liver capsule (Fig. 4g–j). The histotripsy site in animal 8 was in contact with the liver capsule (see below). The histotripsy site in animal 1 was incompletely represented in the section examined, which also suffered from tissue tearing during processing and could not be measured or assessed in terms of relationships with the liver capsule (Supplementary Fig. 2). Surgiflo gel plugs were identified in the samples from animals 8 and 10. The number of 3D Heps aggregates on prepared sections was variable. One aggregate was identified in sectioned obtained from animals 8 and 10, two in animal 4 and three in animals 1 and 2 (Fig. 4d–p; Supplementary Fig. 2). The 3D Heps aggregate in animal 10 appeared to be wedged between the Surgiflo gel plug and the underlying intact liver parenchyma. Two of the three 3D Hep aggregates in animal 8 appeared to be wedged between necrotic parenchyma and the Surgiflo gel plug without a visible interposed intact liver capsule. The remaining eight 3D aggregates in animals 1, 2, 4 and 8 were positioned inside histotripsy sites. The 3D Heps appeared to be mostly viable histologically in test animals 1, 2, 4 and 8, but showed degenerative changes in animal 10. Focal basophilic material

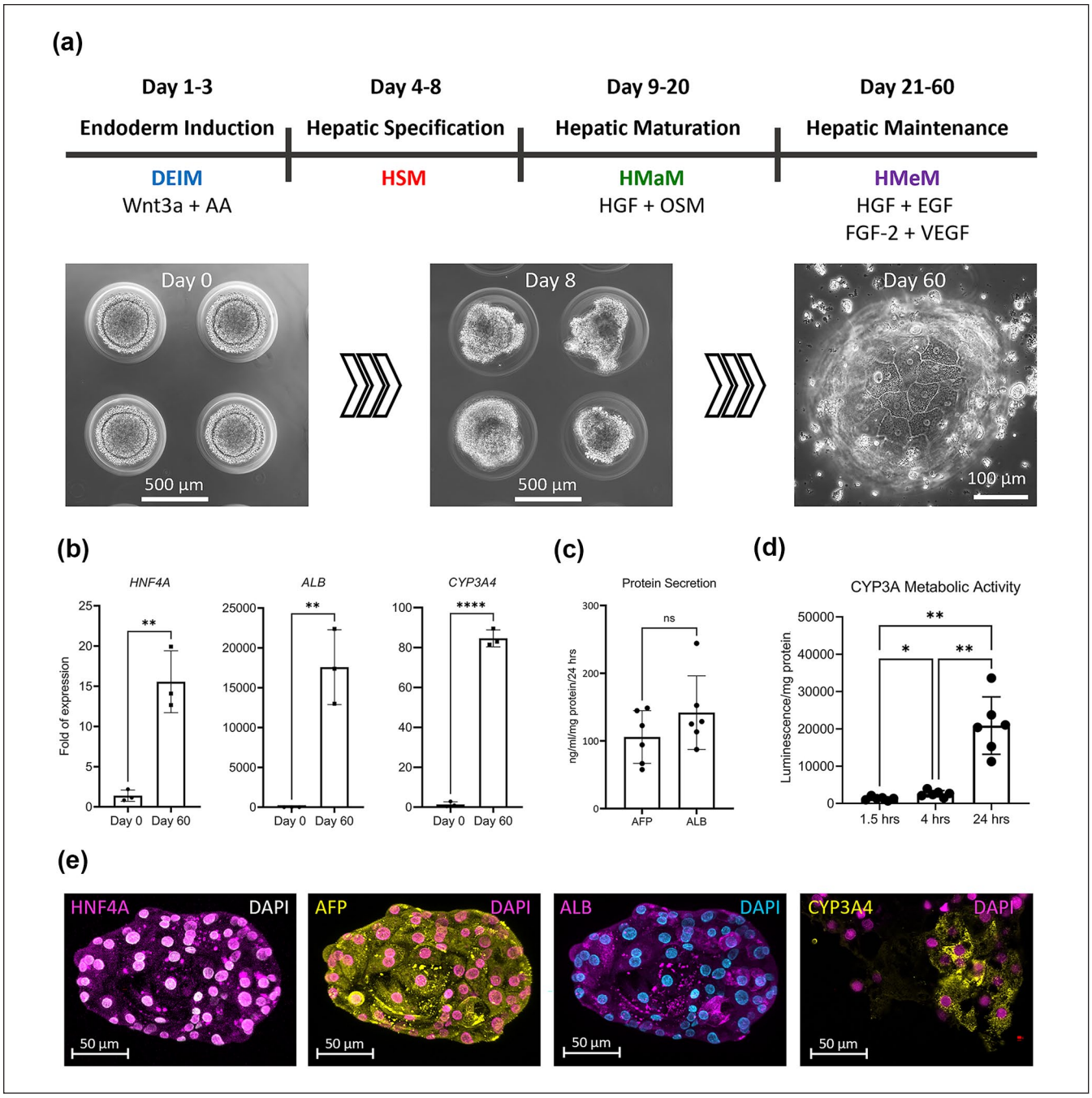

Figure 3. 3D Heps characterisation. (a) A stepwise differentiation protocol was used to generate 3D Heps from hiPSCs. (b) Expression of liver-specific genes HNF4A, ALB and CYP3A4. (c) ELISA was used to measure AFP and ALB secretion by generated 3D Heps. (d) Bioluminescence assay was used to assess CYP3A4 metabolic activity of 3D Heps. (e) Immunostaining was performed to detect liver-specific proteins. DEIM: Definitive Endoderm Induction Medium, HSM: Hepatic Specification Medium, HMaM: Hepatic Maturation Medium, HMeM: Hepatic Maintenance Medium.

present in the 3D Heps in animals 1, 2, 4 and 8 represented probably fragmented nuclei. No inflammatory reaction was identified around the 3D Heps in animals 1, 2 and 4. The histotripsy/injection sites in animals 8 and 10 contained infiltrates of leukocytes. In animal 10, the infiltrate was present between the Surgiflo gel plug, underlying liver parenchyma and a 3D Heps cluster and included a multinucleated giant cell (Fig. 4n–p).

To confirm human origin, immunohistochemical analysis was performed using anti-human nuclei antibody. Stain-positive nuclei was observed only in samples injected with 3D Heps and where cell aggregates were presented with test

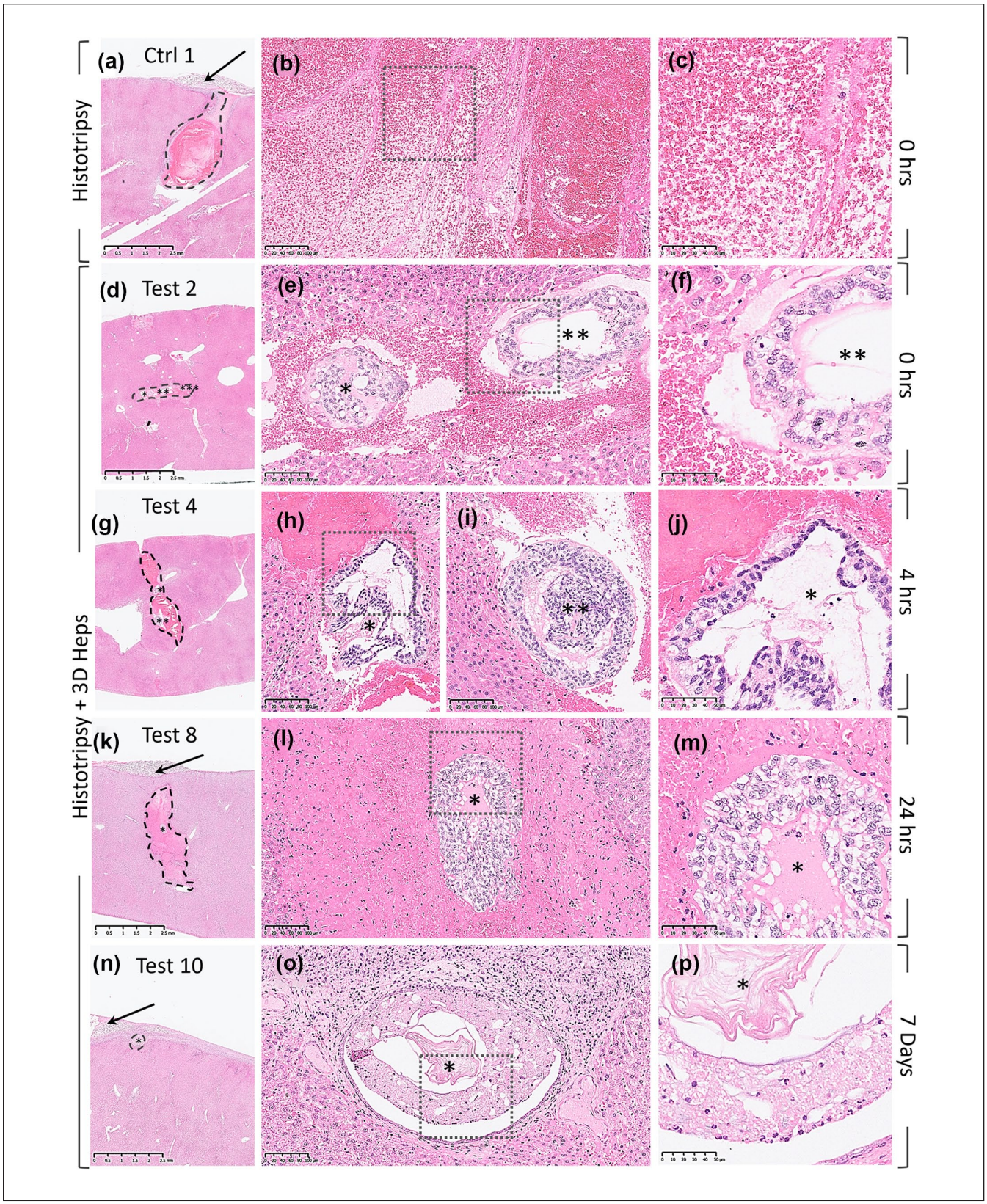

Figure 4. Histological analysis. H&E staining was performed on sections obtained from rat livers following histotripsy (a–c) and 3D Heps transplantation (d–p). Implanted 3D Heps in Test Rat 10 (168 h postimplantation; n–p) was infiltrated with leukocytes (h–i). Cavities are marked with hatched black lines, 3D Heps with asterisks and SURGIFLO with arrows.

10 as exception (Fig. 5). The aggregate identified in test 10 was infiltrated with host immune cells and immunostaining was negative for human nuclei possibly due to degenerative changes (Fig. 5).

Functionality

We performed blood biochemistry on plasma collected from two controls and 10 cell-transplanted rats at the time of termination to detect human AFP and ALB. The collected plasma showed haemolysis in eight samples, of which six were heavily haemolysed. In addition, collected plasma was not sufficient in control rat 1 and cell-transplanted rat 7 to run ALB ELISA (Supplementary Table 1). Human AFP was detected in the plasma of 5 out of the 10 cell-transplanted rats ranging from 0.016 to 1.883 ng/ml. ALB was detected in the plasma of six out of nine transplanted rats ranging from 0.095 to 0.429 ng/ml (Fig. 6; Supplementary Table 1). The detection and detected levels of AFP and ALB bore no correlation with collection time post-implantation. No human AFP or ALB was found in non-transplant control.

Discussion

Cell therapy is a promising approach to treat liver disease; however, the lack of an efficient methodology for cell delivery remains a major bottleneck to the clinical translation of this modality. In this proof-of-concept study, we demonstrate the feasibility of producing a histotripsy cavity within the healthy liver and delivering hPSC-derived liver organoids (3D Heps) into the cavity as a novel approach to the treatment of liver failure in congenital metabolic liver disease.

To assess feasibility, we used a healthy rat animal model as the size of the liver, the tolerance to interventions and the ability to obtain samples for analysis is favourable in comparison with murine models. To allow access and establish direct contact with the ultrasound coupling cone, the liver was exteriorised outside the abdominal cavity. This approach facilitated liver stabilisation as the rodents were not ventilated, with the gauze air trap beneath the liver aiding in reflecting the waves back to the pulse-echo transducer. However, this method posed challenges, including liver stretching that resulted in segment thinning, thereby elevating the risk of liver capsule puncture. Externalisation of the liver also led to visible changes in liver perfusion which may have contributed to the observed 3D Heps leakage in test rats 6 and 7, prior to the application of the haemostat SURGIFLO. The use of a bevelled needle may have contributed to leakage in these instances, either by penetrating too deeply, leading to bleeding and potential capsule damage or by being too shallow, resulting in the leakage of 3D Heps from the syringe. These findings highlight the importance of short-term experiments aimed at identifying procedure-related complications. The local effects of histotripsy on the liver and the nature of the histotripsy contents including the ability to culture hepatocytes from the liquified core of the histotripsy site have previously been reported by our group[30,31].

In human, exteriorisation of the liver will not be required as the delivery of cells can be performed using ultrasound-guided percutaneous or endoscopic injection.

We used histotripsy to create cavities in the liver parenchyma and beneath the liver capsule, providing a suitable niche for cell transplantation. It has been shown previously that the dimensions of the cavity created depend on the ultrasound protocol selected[32]. In a previous publication, we reported the relationship between the dimensions of the cavity and the ultrasound parameters such as the output power and number of pulses employed, for a transducer of similar type[33]. The results presented as Fig. 8 in Pahk et al.[33] were obtained in an optically transparent liver phantom. We further confirmed the production of a cavity of the correct size for a given exposure setting in *ex vivo* chicken liver tissue before applying the same exposure conditions for our *in vivo* experiments. To avoid puncture the liver capsule, the axial length of the cavity required to be smaller than 6 mm, which is the average liver lobe thickness in the male Sprague Dawley rats used in the current study.

By including a pulse-echo transducer, we successfully measured liver lobe thickness in all but two animals enabling precise selection of a sonication site in which the cavity produced would be within liver capsule boundaries and avoid puncturing the liver capsule. Difficulty in assessing thickness of right median lobe in control rat 1 resulted in puncturing the capsule. Subsequently, we reduced the pulse count from 35 to 30 and sonicated rat 2's left median lobe (the only animal to undergo left lobe sonication). Future studies will include real-time imaging for improved procedural monitoring.

Following histotripsy-mediated cell implantation, the animals were recovered in dedicated cages and exhibited expected normal behaviour, physical activity, water consumption, food intake, urination and defecation patterns indicating the method safety. Apart from wound complications in test rats 9 and 10 that were kept for 96 and 168 h post-implantation, the animals maintained a generally healthy appearance. Serum tests for overall rodent and liver health were not conducted during the recovery period. Potential reasons for wound complications include wound trauma by the animals, surgical technique and infection.

Postmortem findings were as would be expected for the animals terminated within 24 h. There was minimal adherence of cavities to adjacent diaphragm/abdominal wall. SURGIFLO, a haemostatic agent, was used on the cavities and has tissue adherence properties. Animals 9 and 10 had a firmer tissue reaction between likely sites of cavity formation and the abdominal wall/diaphragm. This could be a result of xenograft response to injected 3D Heps. Histological analysis indicated that the resulting cavities were around 0.4 $\pm$ 0.1 mm beneath the liver capsule and were around 2.7 $\pm$ 0.7 mm in length and 1.0 $\pm$ 0.3 mm in width.

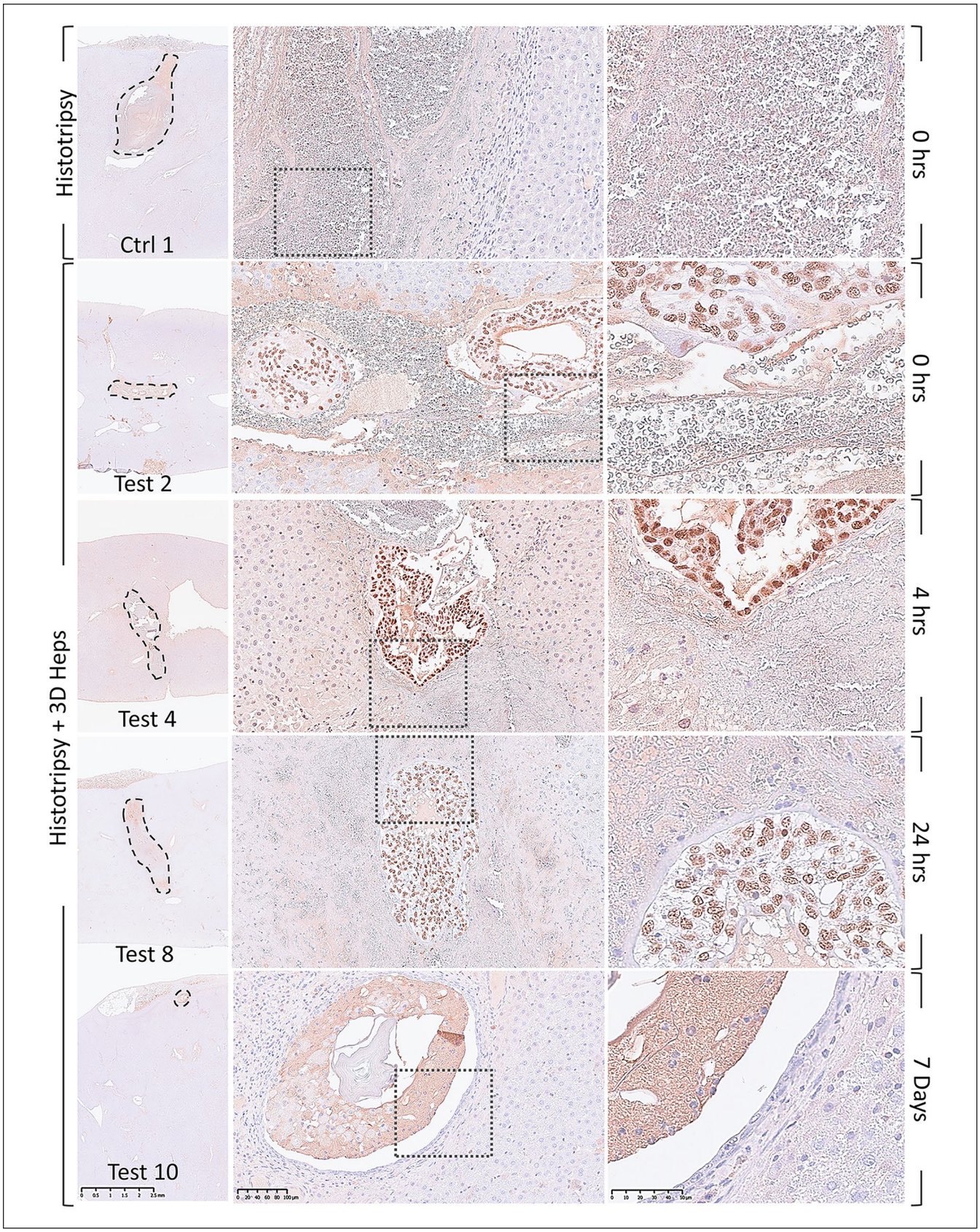

Figure 5. The presence of human 3D Heps was validated using human anti-nuclei antibody. The immunostaining was negative for human nuclei in the aggregate identified in animal 10 possibly due to degenerative changes.

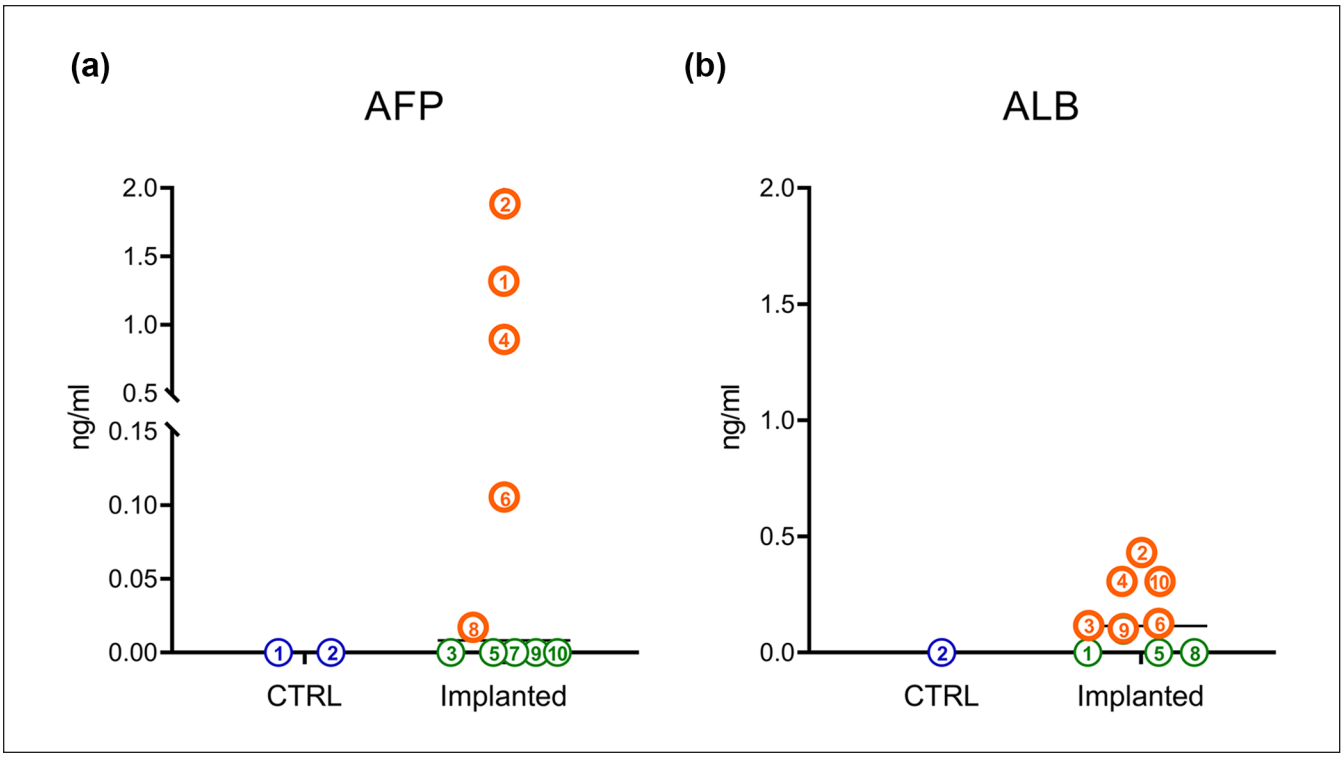

Figure 6. Blood biochemistry analysis. Circulating human AFP was detected in 5 out of 10 cell-transplanted rats. Human ALB was detected in six out of nine cell-transplanted animals. Plasmas positive for AFP and ALB are labelled in orange. The number inside circle shows designated number to rats in control and test groups. Collected serum from Ctrl Rat 1 and Test Rat 7 were not enough to include in ALB ELISA assay. Implanted Test Rats 1 and 2 sacrificed immediately post-implantation; 3 and 4, 4 h post-implantation; 5 and 6, 18 h post-implantation; 7 and 8, 24 h post-implantation; 9, 96 h; and 10, 168 h post-implantation.

In a previous study from our group[26], Matrigel was used to improved retention of transplanted dissociated rat hepatocytes at the site of transplantation. Matrigel is a solubilised basement membrane matrix secreted by Engelberth-Holm-Swarm mouse sarcoma cells which is rich in laminin and collagen-IV. As Matrigel turns into gel at temperatures between 22°C and 37°C, it is a suitable protein carrier to improve cell retention at the site of transplantation. However, as an undefined animal product, its application in clinical practice risks the transfer of animal pathogens and we therefore avoided its use in the development of this platform for clinical translation.

The use of mature hepatocytes was avoided as they are prone to cell death, epithelial-to-mesenchymal (EMT) transition and loss of functionality following dissociation[34]. In this study, we transplanted undissociated hiPSC-derived 3D liver organoids (3D Heps) to circumvent EMT and cell death. However, the size of 3D Heps at around 200–300 μm in diameter made it more difficult to implant in comparison with the smaller dissociated hepatocytes. Creating small cavities beneath the liver capsule imposed difficulties in visual identification of the generated cavities and implantation of undissociated 3D-Heps with accuracy. On histology of the explanted livers, we successfully identified 5 out of 10 generated cavities and confirmed the presence of implanted human 3D Heps using anti-human nuclei antibody. The presence of functional human cells was supported by the finding of human AFP and albumin in the blood sampled at termination only in the cell transplant animals. The detection of human AFP and ALB in the serum suggests viable implanted cells but requires validation as both proteins are relatively stable and can be released from damaged cells post-implantation.

In summary, we have obtained encouraging early feasibility data on histotripsy-mediated cell transplantation as a potential method of cell therapy for some of the congenital metabolic liver disease. While demonstrating short-term safety of the methodology, ongoing work will focus on long-term cell integration and functionality and assessment of the therapeutic efficacy. Low thickness of rat liver imposes limitation in number and size of the cavities that can be created and as a result the number of cells that can be transplanted; however, this would not be an issue following translation of the technique into human as larger cavities can be generated to transplant larger number of cells. In addition, the procedure can be performed percutaneously in human using ultrasound-guided cell implantation to avoid laparotomy and making the procedure less invasive.

ORCID iD

Hassan Rashidi https://orcid.org/0000-0001-8078-6688

Research ethics and patient consent

This study involved only pre-clinical research conducted in animal models. All procedures were carried out in compliance with relevant ethical guidelines and approved by the appropriate institutional Animal Welfare and Ethical Review Body (AWERB). The study was performed under a valid personal and project license, in accordance with the regulations set forth by the Animals (Scientific Procedures) Act 1986 and the EU Directive 2010/63/EU on the protection of animals used for scientific purposes. No patient samples were used, and no human participants were involved in this study; therefore, patient consent was not required.

Author contributions

H.R. contributed to the conceptualisation, secured the grant, performed the experiments, analysed and compiled the data, and wrote the manuscript. A.K. and S.F. performed experiments and contributed to the writing and editing of the manuscript. A.H. analysed samples and contributed to editing the manuscript. P.G. contributed to editing the manuscript. A.Q., B.D. and N.S. were involved in the conceptualisation, securing the grant and contributing to the writing and editing of the manuscript.

Funding

The author(s) disclosed receipt of the following financial support for the research, authorship and/or publication of this article: This work is supported by 2020\100261 Seedcorn Award from Rosetrees Trust and The Wellington Hospital, HCA London. H.R. is funded by the National Institute for Health Research (NIHR) GOSH Biomedical Research Center (BRC). A.Q. is supported by the NIHR UCLH/UCL BRC.

Declaration of conflicting interests

The author(s) declared the following potential conflicts of interest with respect to the research, authorship and/or publication of this article: H.R. is the founder of Auxi Bio Ltd; however, the activities of the company are not related to the research presented in this study. The other authors declare no conflict of interest related to this work.

Statement of human and animal rights

This article does not contain any studies with human or animal subjects.

Statement of informed consent

There are no human subjects in this article and informed consent is not applicable.

Data availability statement

The data and materials supporting the findings of this study are available from the corresponding author upon reasonable request. All relevant datasets generated and analysed during the study are included in the manuscript and/or its h.rashidi@ucl.ac.ukary information files, where applicable.

Supplemental material

Supplemental material for this article is available online.

References

1. Scorza M, Elce A, Zarrilli F, Liguori R, Amato F, Castaldo G. Genetic diseases that predispose to early liver cirrhosis. *Int J Hepatol*. 2014;2014:713754. doi:10.1155/2014/713754.
2. Vakili O, Mafi A, Pourfarzam M. Liver disorders caused by inborn errors of metabolism. *Endocr Metab Immune Disord Drug Targets*. 2024;24(2):194–207. doi:10.2174/1871530323666230623120935.
3. Khalil A, Quaglia A, Gélat P, Saffari N, Rashidi H, Davidson B. New developments and challenges in liver transplantation. *J Clin Med*. 2023;12(17):5586.
4. Alwahsh SM, Rashidi H, Hay DC. Liver cell therapy: is this the end of the beginning? *Cell Mol Life Sci*. 2018;75(8):1307–24. doi:10.1007/s00018-017-2713-8.
5. Ghasemzad M, Hashemi M, Lavasani ZM, Hossein-Khannazer N, Bakhshandeh H, Gramignoli R, Keshavarz Alikhani H, Najimi M, Nikeghbalian S, Vosough M. Novel gene-correction-based therapeutic modalities for monogenic liver disorders. *Bioengineering*. 2022;9(8):392.
6. Zeilinger K, Freyer N, Damm G, Seehofer D, Knöspel F. Cell sources for in vitro human liver cell culture models. *Exp Biol Med (Maywood)*. 2016;241(15):1684–98. doi:10.1177/1535370216657448.
7. Alhaque S, Themis M, Rashidi H. Three-dimensional cell culture: from evolution to revolution. *Philos Trans R Soc Lond B Biol Sci*. 2018;373(1750):20170216. doi:10.1098/rstb.2017.0216.
8. Hay DC, Zhao D, Ross A, Mandalam R, Lebkowski J, Cui W. Direct differentiation of human embryonic stem cells to hepatocyte-like cells exhibiting functional activities. *Cloning Stem Cells*. 2007;9(1):51–62. doi:10.1089/clo.2006.0045.
9. Agarwal S, Holton KL, Lanza R. Efficient differentiation of functional hepatocytes from human embryonic stem cells. *Stem Cells*. 2008;26(5):1117–27. doi:10.1634/stemcells.2007-1102.
10. Takebe T, Sekine K, Enomura M, Koike H, Kimura M, Ogaeri T, Zhang RR, Ueno Y, Zheng YW, Koike N, Aoyama S, et al. Vascularized and functional human liver from an iPSC-derived organ bud transplant. *Nature*. 2013;499(7459):481–484. doi:10.1038/nature12271.
11. Hu H, Gehart H, Artegiani B, López-Iglesias C, Dekkers F, Basak O, van Es J, Chuva de Sousa Lopes SM, Begthel H, Korving J, van den Born M, et al. Long-term expansion of functional mouse and human hepatocytes as 3D organoids. *Cell*. 2018;175(6):1591–1606.e19. Doi:10.1016/j.cell.2018.11.013.
12. Rashidi H, Luu NT, Alwahsh SM, Ginai M, Alhaque S, Dong H, Tomaz RA, Vernay B, Vigneswara V, Hallett JM, Chandrashekran A, et al. 3D human liver tissue from pluripotent stem cells displays stable phenotype in vitro and supports compromised liver function in vivo. *Arch Toxicol*. 2018;92(10):3117–29. doi:10.1007/s00204-018-2280-2.
13. Tomaz RA, Zacharis ED, Bachinger F, Wurmser A, Yamamoto D, Petrus-Reurer S, Morell CM, Dziedzicka D, Wesley BT, Geti I, Segeritz C-P, et al. Generation of functional hepatocytes by forward programming with nuclear receptors. *Elife*. 2022;11:e71591. doi:10.7554/eLife.71591.

14. Strom SC, Fisher RA, Thompson MT, Sanyal AJ, Cole PE, Ham JM, Posner MP. Hepatocyte transplantation as a bridge to orthotopic liver transplantation in terminal liver failure. *Transplantation*. 1997;63(4):559–69. doi:10.1097/00007890-199702270-00014.
15. Dhawan A, Puppi J, Hughes RD, Mitry RR. Human hepatocyte transplantation: current experience and future challenges. *Nat Rev Gastroenterol Hepatol*. 2010;7(5):288–98. doi:10.1038/nrgastro.2010.44.
16. Komori J, Boone L, DeWard A, Hoppo T, Lagasse E. The mouse lymph node as an ectopic transplantation site for multiple tissues. *Nat Biotechnol*. 2012;30(10):976–83. doi:10.1038/nbt.2379.
17. Dwyer BJ, Macmillan MT, Brennan PN, Forbes SJ. Cell therapy for advanced liver diseases: repair or rebuild. *J Hepatol*. 2021;74(1):185–99. doi:10.1016/j.jhep.2020.09.014.
18. Gramignoli R, Vosough M, Kannisto K, Srinivasan RC, Strom SC. Clinical hepatocyte transplantation: practical limits and possible solutions. *Eur Surg Res*. 2015;54(3–4):162–77. doi:10.1159/000369552.
19. Gupta S, Rajvanshi P, Sokhi R, Slehria S, Yam A, Kerr A, Novikoff PM. Entry and integration of transplanted hepatocytes in rat liver plates occur by disruption of hepatic sinusoidal endothelium. *Hepatology*. 1999;29(2):509–19. doi:10.1002/hep.510290213.
20. Joseph B, Malhi H, Bhargava KK, Palestro CJ, McCuskey RS, Gupta S. Kupffer cells participate in early clearance of syngeneic hepatocytes transplanted in the rat liver. *Gastroenterology*. 2002;123(5):1677–85. doi:10.1053/gast.2002.36592.
21. Malhi H, Annamaneni P, Slehria S, Joseph B, Bhargava KK, Palestro CJ, Novikoff PM, Gupta S. Cyclophosphamide disrupts hepatic sinusoidal endothelium and improves transplanted cell engraftment in rat liver. *Hepatology*. 2002;36(1):112–21. doi:10.1053/jhep.2002.33896.
22. Slehria S, Rajvanshi P, Ito Y, Sokhi RP, Bhargava KK, Palestro CJ, McCuskey RS, Gupta S. Hepatic sinusoidal vasodilators improve transplanted cell engraftment and ameliorate microcirculatory perturbations in the liver. *Hepatology*. 2002;35(6):1320–28. doi:10.1053/jhep.2002.33201.
23. Yamanouchi K, Zhou H, Roy-Chowdhury N, Macaluso F, Liu L, Yamamoto T, Yannam GR, Enke C, Solberg TD, Adelson AB, Platt JL, et al. Hepatic irradiation augments engraftment of donor cells following hepatocyte transplantation. *Hepatology*. 2009;49(1):258–67. doi:10.1002/hep.22573.
24. Aubry JF, Pauly KB, Moonen C, Haar GT, Ries M, Salomir R, Sokka S, Sekins KM, Shapira Y, Ye F, Huff-Simonin H, et al. The road to clinical use of high-intensity focused ultrasound for liver cancer: technical and clinical consensus. *J Ther Ultrasound*. 2013;1:13. doi:10.1186/2050-5736-1-13.
25. Khokhlova TD, Hwang JH. HIFU for palliative treatment of pancreatic cancer. *Adv Exp Med Biol*. 2016;880:83–95. doi:10.1007/978-3-319-22536-4_5.
26. Pahk KJ, Mohammad GH, Malago M, Saffari N, Dhar DK. A novel approach to ultrasound-mediated tissue decellularization and intra-hepatic cell delivery in rats. *Ultrasound Med Biol*. 2016;42(8):1958–67. doi:10.1016/j.ultrasmedbio.2016.03.020.
27. Rashidi H, Leong YC, Venner K, Pramod H, Fei QZ, Jones OJR, Moulding D, Sowden JC. Generation of 3D retinal tissue from human pluripotent stem cells using a directed small molecule-based serum-free microwell platform. *Sci Rep*. 2022;12(1):6646. doi:10.1038/s41598-022-10540-1.
28. Lucendo-Villarin B, Rashidi H, Alhaque S, Fischer L, Meseguer-Ripolles J, Wang Y, O'Farrelly C, Themis M, Hay DC. Serum free production of three-dimensional human hepatospheres from pluripotent stem cells. *J Vis Exp*. 2019;(149):10.3791/59965. doi:10.3791/59965.
29. Soneson JE. Extending the utility of the parabolic approximation in medical ultrasound using wide-angle diffraction modeling. *IEEE Trans Ultrason Ferroelectr Freq Control*. 2017;64(4):679–87. doi:10.1109/tuffc.2017.2654125.
30. Froghi S, de Andrade MO, Hadi LM, Gelat P, Rashidi H, Quaglia A, Fuller B, Saffari N, Davidson B. Liver ultrasound histotripsy: novel analysis of the histotripsy site cell constituents with implications for histotripsy application in cell transplantation and cancer therapy. *Bioengineering*. 2023;10(2):276. doi:10.3390/bioengineering10020276.
31. Froghi S, Hall A, Hanafi Bin Jalal A, Oliveira de Andrade M, Hadi LM, Rashidi H, Gélat P, Saffari N, Davidson B, Quaglia A. Ultrasound histotripsy on a viable perfused whole porcine liver: histological aspects, including 3D reconstruction of the histotripsy site. *Bioengineering (Basel)*. 2023;10(3):278. doi:10.3390/bioengineering10030278.
32. Pahk KJ, de Andrade MO, Gélat P, Kim H, Saffari N. Mechanical damage induced by the appearance of rectified bubble growth in a viscoelastic medium during boiling histotripsy exposure. *Ultrason Sonochem*. 2019;53:164–77. doi:10.1016/j.ultsonch.2019.01.001.
33. Pahk KJ, Gélat P, Sinden D, Dhar DK, Saffari N. Numerical and experimental study of mechanisms involved in boiling histotripsy. *Ultrasound Med Biol*. 2017;43(12):2848–61. doi:10.1016/j.ultrasmedbio.2017.08.938.
34. Cicchini C, Amicone L, Alonzi T, Marchetti A, Mancone C, Tripodi M. Molecular mechanisms controlling the phenotype and the EMT/MET dynamics of hepatocyte. *Liver Int*. 2015;35(2):302–10. doi:10.1111/liv.12577.